

Electronic Supplementary Information for

A new air- and moisture-stable pentagonal-bipyramidal Dy^{III} single-ion magnet based on HMPA ligand

Lei-Lei Li*, Hong-Dan Su, Shuang Liu*, Ya-Chao Xu and Wen-Zhen Wang

*School of Chemistry and Chemical Engineering, Xi'an Shiyou University, Xi'an
710065, China.*

Email: lll@xsysu.edu.cn; liush@xsysu.edu.cn

Contents:

1. Crystal data and structure	2;
2. PXRD patterns and IR spectrum	5;
3. Other magnetic data	6;
4. References	15;

1. Crystal data and structure

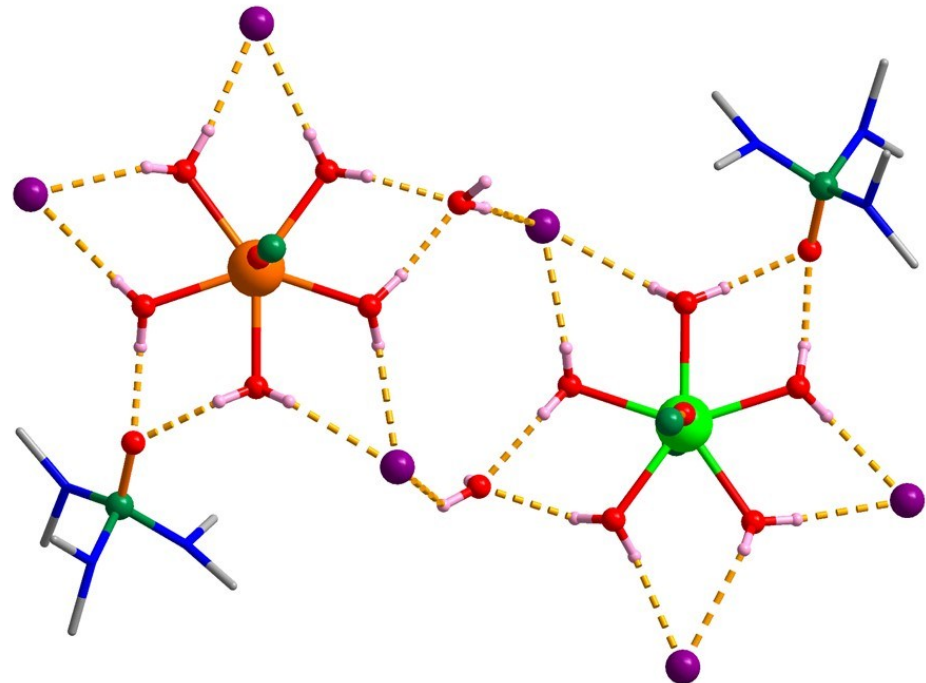


Fig S1. The hydrogen bonds between coordinated H_2O molecules and free solvents, free ligands and Br^- ions. Color codes: O red, H pink, N blue, C gray, P green, Br violet

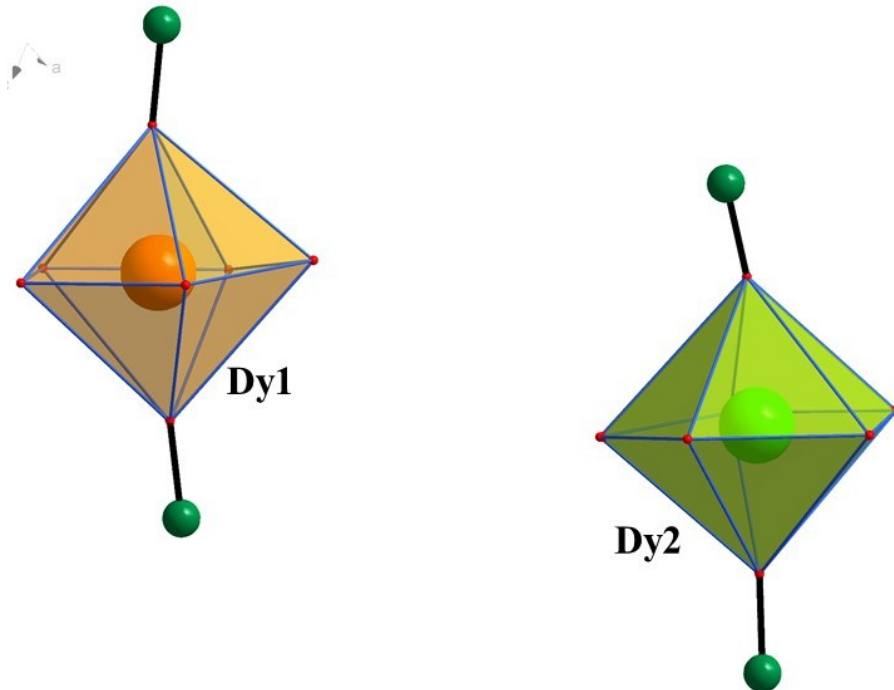


Fig S2. Coordination polyhedrons of Dy^{III} centers. Colour codes: O red, P green.

Table S1. Selected bonds and angles for complex **1**

1			
Bonds/Angles	Å/°	Bonds/Angles	Å/°
Dy1-O6	2.195(8)	O17-Dy1-O13	143.8(3)
Dy1-O7	2.228(9)	O17-Dy1-O19	143.5(3)
Dy1-O12	2.347(8)	O17-Dy1-O20	71.2(3)
Dy1-O13	2.383(8)	O19-Dy1-O13	72.5(3)
Dy1-O17	2.334(8)	O20-Dy1-O12	142.4(3)
Dy1-O19	2.371(9)	O20-Dy1-O13	144.6(3)
Dy1-O20	2.337(8)	O20-Dy1-O19	72.3(3)
Dy2-O5	2.218(8)	O5-Dy2-O9	176.9(3)
Dy2-O9	2.224(9)	O5-Dy2-O11	89.0(3)
Dy2-O11	2.368(8)	O5-Dy2-O14	89.9(4)
Dy2-O14	2.362(10)	O5-Dy2-O15	90.7(3)
Dy2-O15	2.346(8)	O5-Dy2-O16	86.0(3)
Dy2-O16	2.368(9)	O5-Dy2-O1	91.8(3)
Dy2-O1	2.351(8)	O9-Dy2-O11	89.1(3)
O6-Dy1-O7	177.8(3)	O9-Dy2-O14	93.1(4)
O6-Dy1-O12	87.4(3)	O9-Dy2-O15	89.4(3)
O6-Dy1-O13	92.7(3)	O9-Dy2-O16	91.1(3)
O6-Dy1-O17	92.0(3)	O9-Dy2-O1	89.9(3)
O6-Dy1-O19	88.8(4)	O11-Dy2-O16	72.1(3)
O6-Dy1-O20	90.3(3)	O14-Dy2-O11	144.2(3)
O7-Dy1-O12	90.5(3)	O14-Dy2-O16	143.4(3)
O7-Dy1-O13	86.1(3)	O15-Dy2-O11	144.4(3)
O7-Dy1-O17	88.0(3)	O15-Dy2-O14	71.4(3)
O7-Dy1-O19	92.5(4)	O15-Dy2-O16	72.3(3)
O7-Dy1-O20	91.8(3)	O15-Dy2-O1	144.0(3)
O12-Dy1-O13	73.0(3)	O1-Dy2-O11	71.5(3)
O12-Dy1-O19	145.0(3)	O1-Dy2-O14	72.7(3)
O17-Dy1-O12	71.4(3)	O1-Dy2-O16	143.6(3)

Table S2. Continuous Shape Measures (CshM)^[1] calculation for complex 1

Structure	HP-7	HPY-7	PBPY-7	COC-7	CTPR-7	JPBY-7	JETPY-7
Dy1	34.232	25.269	0.196	7.568	5.785	2.789	23.472
Dy2	34.314	24.936	0.114	7.923	6.046	2.701	24.612

HP-7 = Heptagon (D_{7h}); HPY-7 = Hexagonal pyramid (C_{6v}); PBPY-7 = Pentagonal bipyramid (D_{5h}); COC-7 = Capped octahedron (C_{3v}); CTPR-7 = Capped trigonal prism (C_{2v}); JPBY-7 = Johnson pentagonal bipyramid J13 (D_{5h}); JETPY-7 = Johnson elongated triangular pyramid J7 (C_{3v}).

Table S3. Comparison of selected crystallography parameters of **1** with other phosphine oxide based SIMs

complex	Average axial Dy-O bond length (Å)	Average equatorial Dy-Ow bond length (Å)	Angle of axial O-Dy-O (°)	Deviation from ideal D_{5h} symmetry	U_{eff} (diluted sample) (K)
[Dy(Cy ₃ PO) ₂ (H ₂ O) ₅]Br ₃ ·2(Cy ₃ PO)·2H ₂ O·2EtOH ^[2]	2.200	2.352	179.04	0.142	543(-) ^a
[Dy(Cy ₃ PO) ₂ (H ₂ O) ₅]Cl ₃ ·(Cy ₃ PO)·H ₂ O·EtOH ^[2]	2.219	2.359	175.79	0.239	472(-) ^a
[Dy(^t BuPO(NH ^t Pr ₂)) ₂ (H ₂ O) ₅]I ₃ ·(^t BuPO(NH ^t Pr ₂))·H ₂ O ^[3]	2.206	2.364	175.14	0.224	651(735.4)
[Dy(CyPh ₂ PO) ₂ (H ₂ O) ₅]Br ₃ ·2(Cy ₃ PO)·3H ₂ O·EtOH ^[4]	2.217	2.364	174.2	0.174	508(467)
Dy1	2.219	2.349	175.6	0.154	460(-)
Dy2	2.219	2.348	176.7	0.284	
[Dy(HMPA) ₂ (H ₂ O) ₅]I ₃ ·2HMPA ^[5]	2.205	2.360	178.0	0.131	600(-)
1-Dy1	2.212	2.354	177.8	0.196	556(550)
1-Dy2	2.221	2.359	176.9	0.114	

^a The author stated the dilution sample had similar ac susceptibility pattern with the pure sample.

2. PXRD patterns and IR spectrum

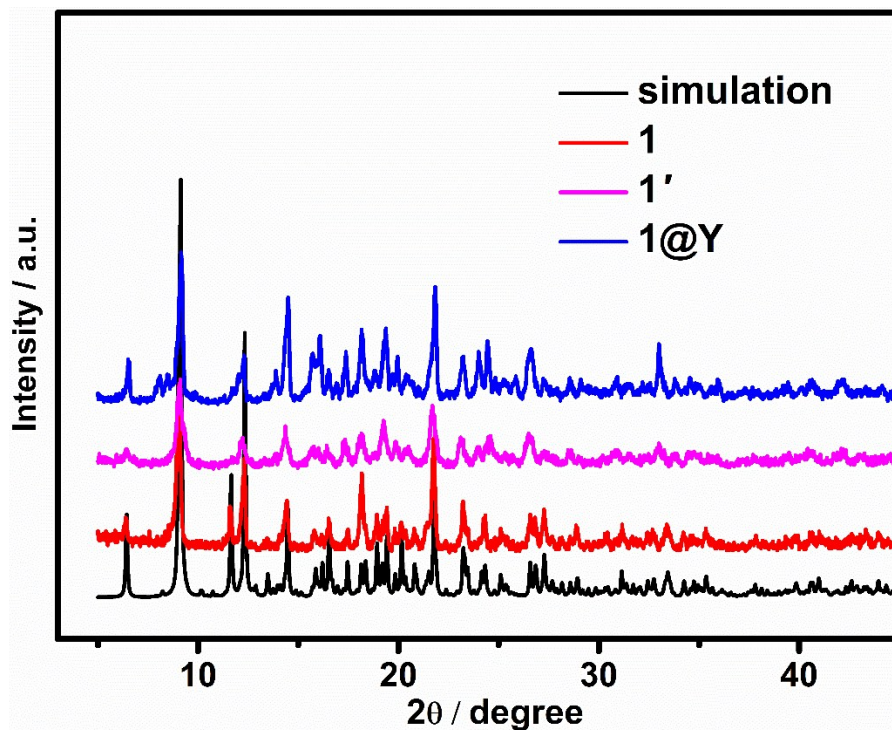


Fig S3. Comparison of the experimental PXRD pattern of **1**, **1'** and **1@Y** with the simulated one from the single crystal data of **1**. **1'** was tested after kept in a glass vial at ordinary condition for *ca.* seven months without inert-gas protection or any special measures.

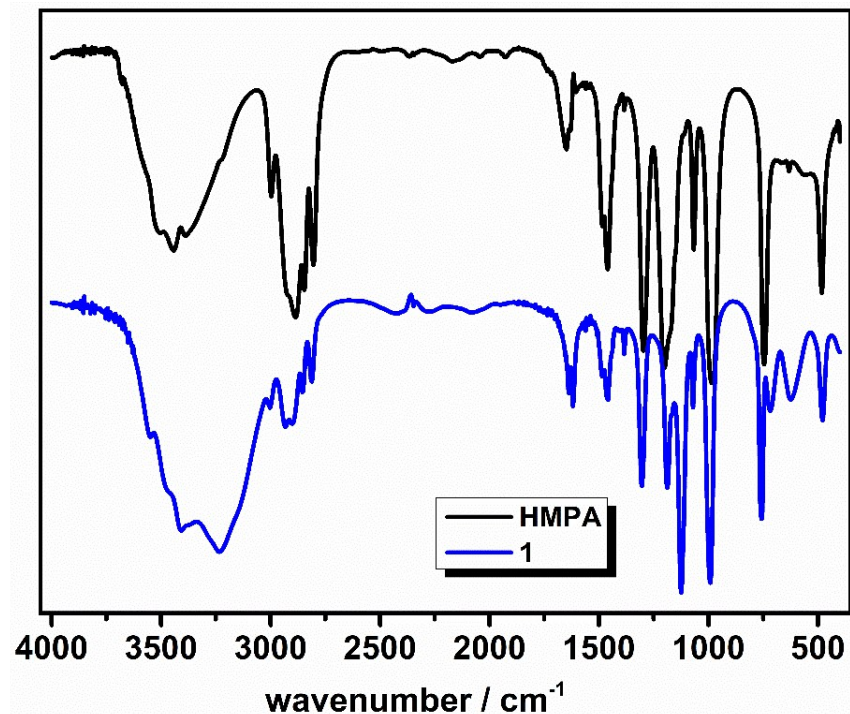


Fig S4. The IR spectrum of **1** and HM

3. Other magnetic data

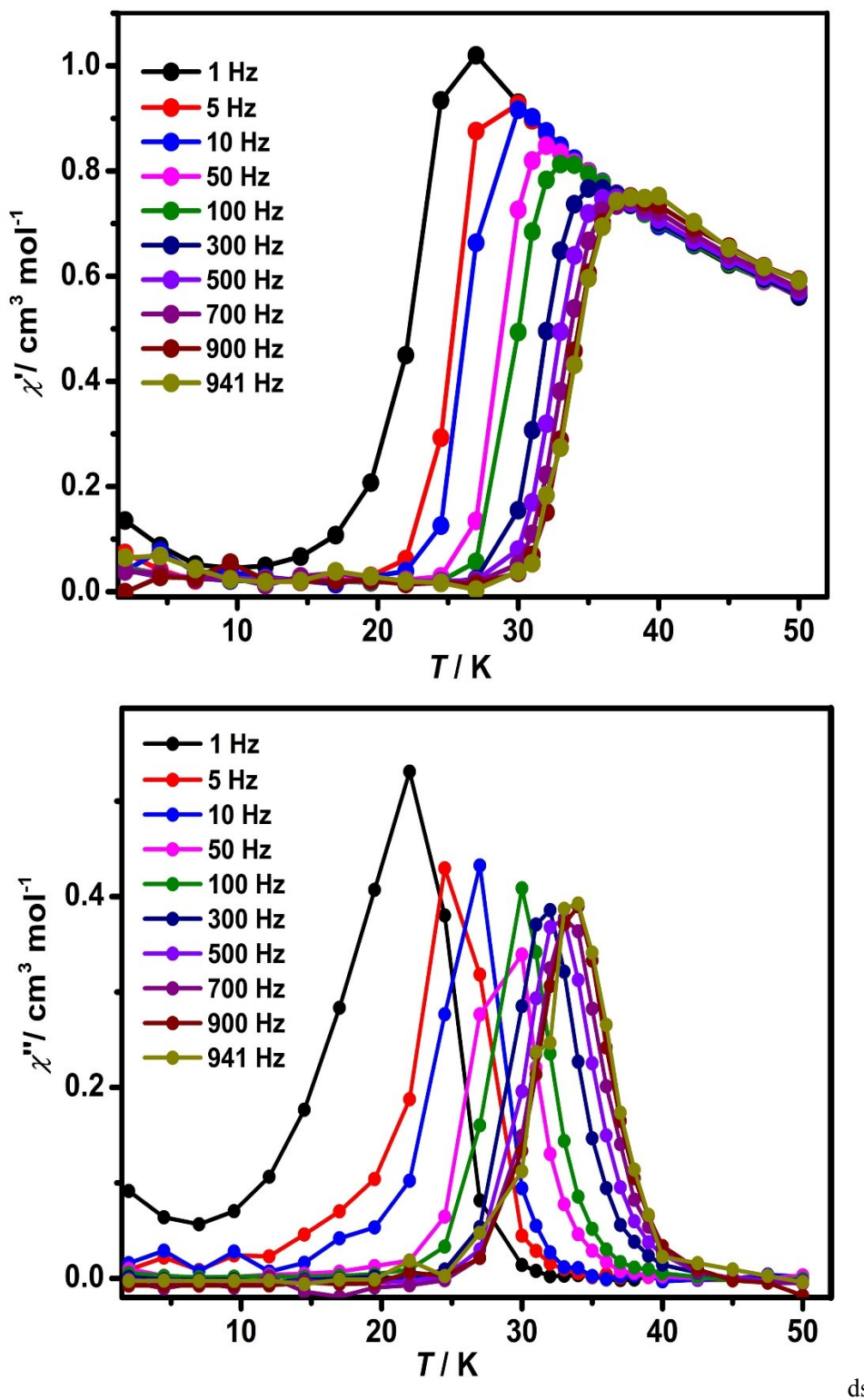


Fig S5. In-phase (top) and out-of-phase (bottom) components of variable-temperature ac susceptibility of **1** under zero dc field. The solid lines are guides for eyes.

Table S4. The best fitting parameters for Cole-Cole plots of **1** under zero applied dc field.

T (K)	χ_s	χ_t	τ (s)	α
20	0.0180813	1.12818	0.309932	0.0136141
21	0.0175817	1.31656	0.302864	0.0418059
22	0.017144	1.2751	0.215238	0.0429817
23	0.016392	1.24585	0.14129	0.052536
24	0.0138342	1.2216	0.0833704	0.0706592
25	0.0126073	1.1853	0.0440235	0.0828304
26	0.0122267	1.14254	0.0219444	0.084406
27	0.011026	1.10025	0.0107135	0.0853662
28	0.00949227	1.05991	0.00531943	0.0839113
29	0.00939185	1.02249	0.00270571	0.0816184
30	0.00360095	0.987629	0.0014146	0.0789837
31	9.84069E-16	0.956308	7.64871E-4	0.0745778
32	2.18111E-15	0.925174	4.30026E-4	0.0638014
33	6.89439E-16	0.895847	2.50864E-4	0.0434504
34	4.61974E-32	0.875001	1.51793E-4	0.0563724
35	7.09848E-32	0.846085	9.78859E-5	4.32305E-10
36	1.03409E-31	0.826617	6.37915E-5	4.52927E-10

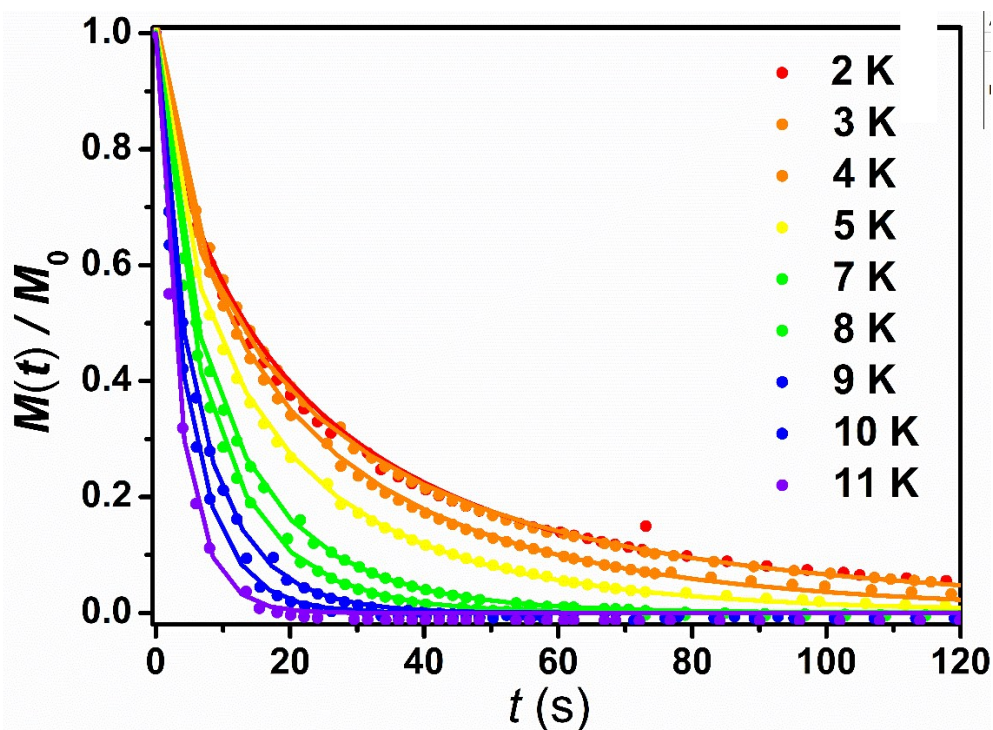


Fig S6. Normalized dc magnetic relaxation data for **1** under the final zero dc field. The solid lines are fits using $M(t) = M_f + (M_f - M_0) \exp[-(t/\tau)^\beta]$ (τ , relaxation time; $M(t)$, magnetization at time t ; M_f , the final magnetization at $t = \infty$; M_0 , magnetization at $t = 0$; β , a free variable).

Table S5. The best fitting results for dc magnetic relaxation data for **1** under zero applied dc field.

T (K)	M_0/M_0	M_f/M_0	τ (s)	β
2	1.02473	0.00421	20.3535	0.64684
3	1.02762	0.00397	21.45572	0.68495
4	1.02137	0.00032695	18.20233	0.70888
5	1.01075	6.81356E-23	13.89797	0.72386
7	1.0028	1.13724E-32	9.58285	0.81689
8	1.00026	1.22968E-22	7.8238	0.85959
9	0.99986	1.48445E-23	6.10766	0.88554
10	0.99971	3.96581E-25	4.77086	0.92493
11	0.99932	1.21215e-24	3.46552	0.94468

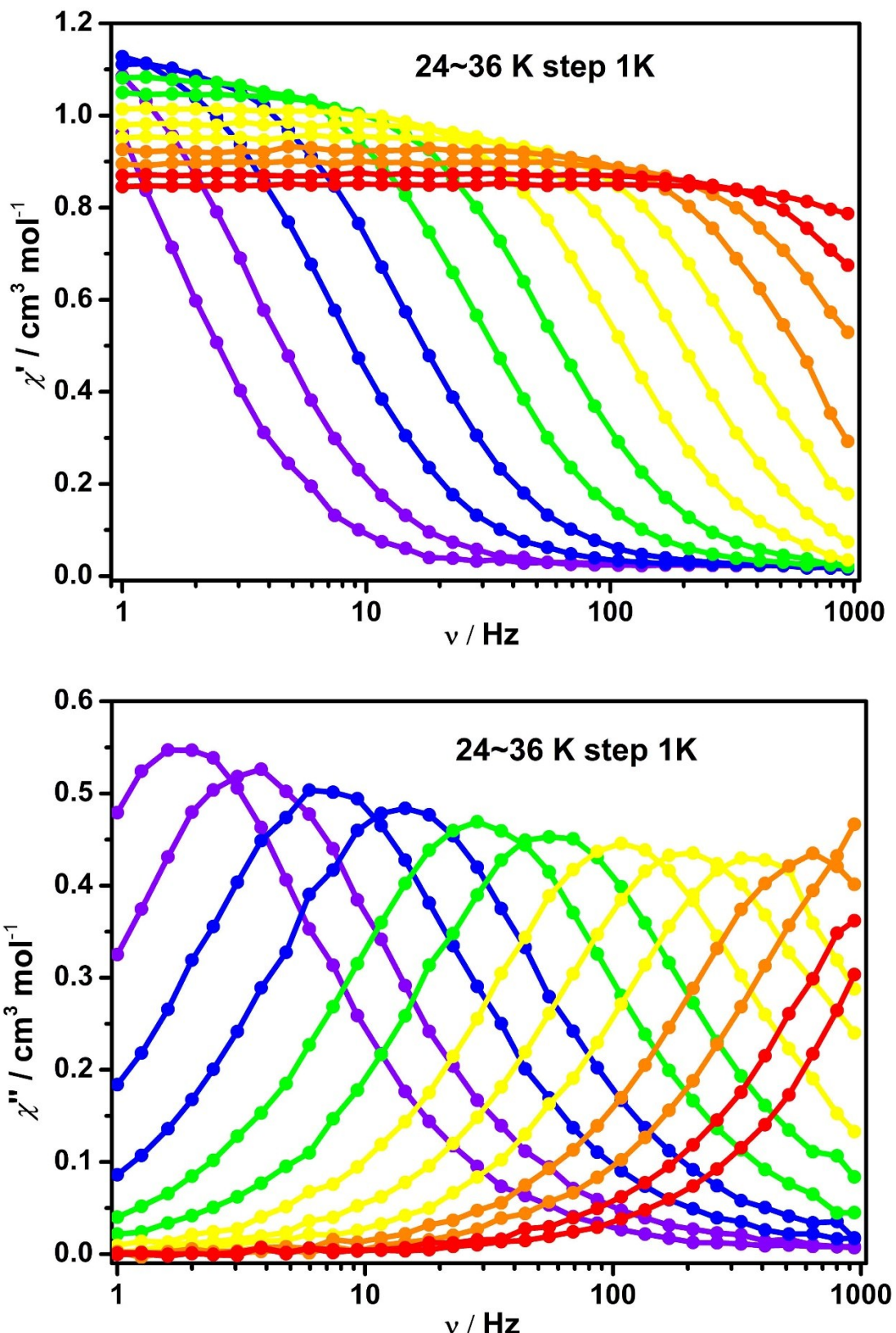


Fig S7. In-phase (top) and put-of-phase (bottom) components of variable-frequency ac susceptibility of **1** under 1200 Oe dc field.

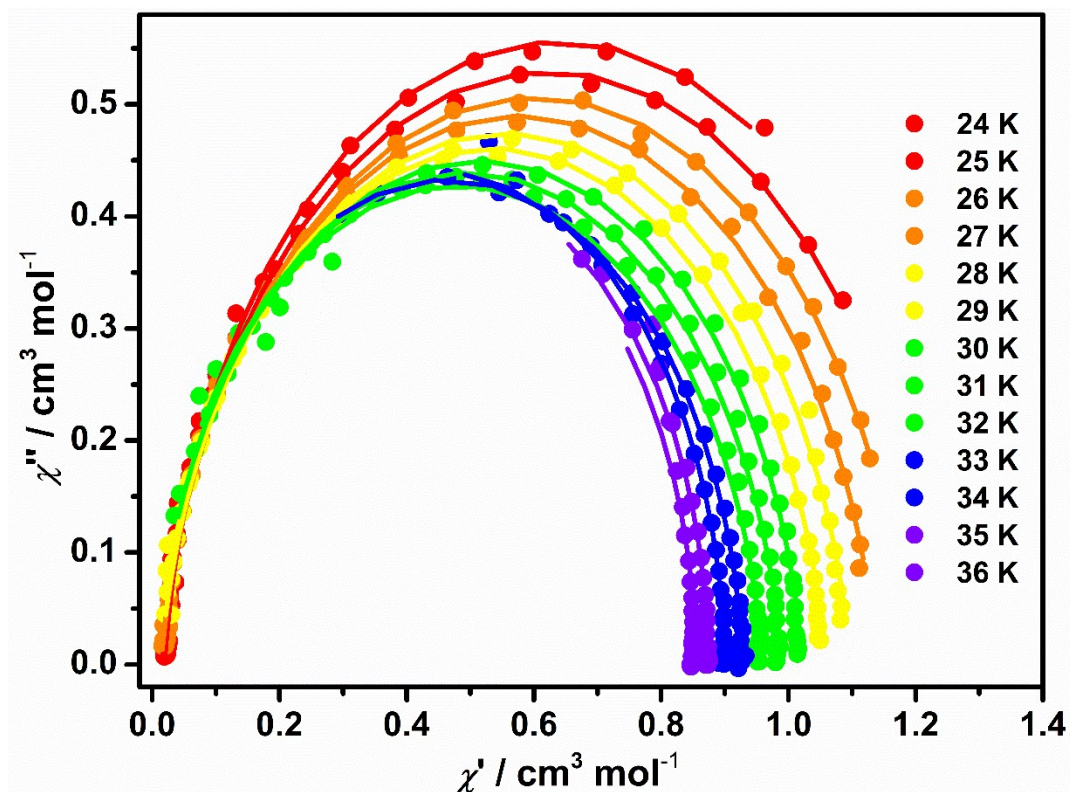


Fig S8. Cole-Cole plots for **1** under 1200 Oe dc field. The solid lines represent the best fitting results using Debye mode.

Table S6. The best fitting parameters for Cole-Cole plots of **1** under 1200 Oe applied dc field

T (K)	χ_s	χ_t	τ (s)	α
24	0.0191384	1.2626	0.0847527	0.071032
25	0.015884	1.22945	0.0455386	0.0867322
26	0.0135576	1.18861	0.0226638	0.0943448
27	0.0135171	1.13865	0.0110128	0.0877455
28	0.0131759	1.0968	0.00544843	0.0843537
29	0.00887373	1.05778	0.0027657	0.0817149
30	0.00660415	1.02166	0.00145054	0.0767424
31	1.43263E-16	0.988882	7.79334E-4	0.0752084
32	1.34492E-16	0.959081	4.42432E-4	0.0721931
33	2.30371E-17	0.927856	2.61368E-4	0.0441084
34	6.29411E-18	0.899305	1.53519E-4	0.0149175
35	1.255E-17	0.873192	9.70537E-5	0.00426391
36	4.46166E-17	0.853373	6.38201E-5	1.89805E-11

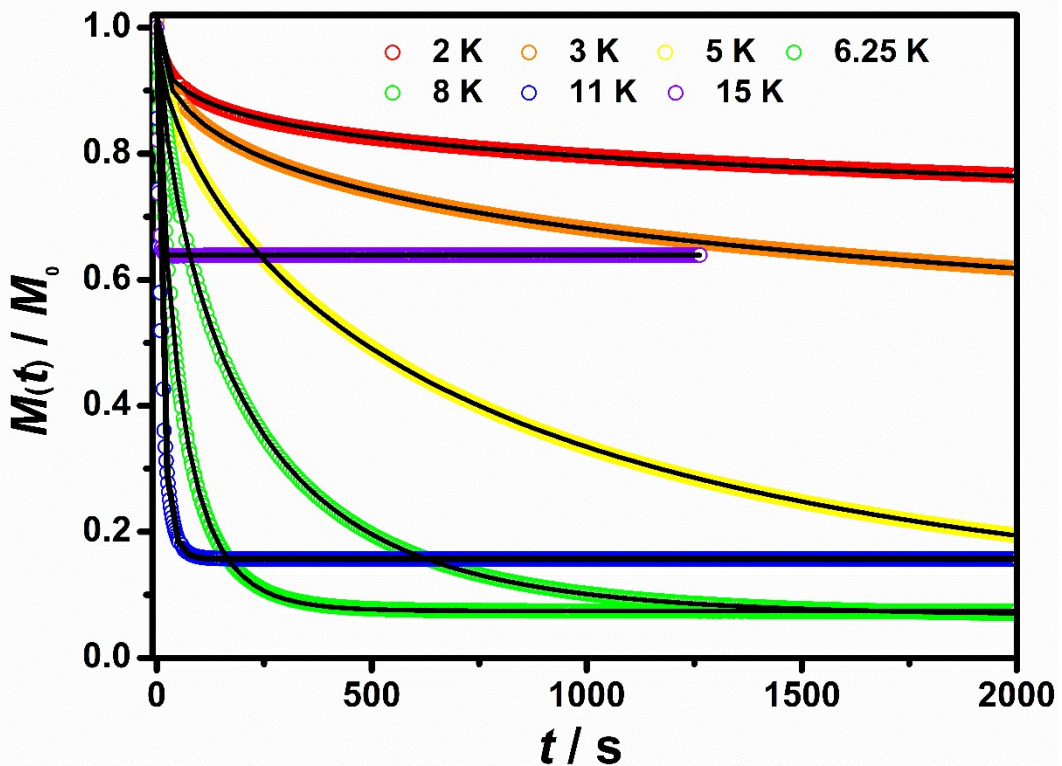


Fig S9. Normalized dc magnetic relaxation data for **1** under the final 1200 Oe dc field. The solid lines are fits using $M(t) = M_f + (M_f - M_0) \exp[-(t/\tau)^\beta]$ (τ , relaxation time; $M(t)$, magnetization at time t ; M_f , the final magnetization at $t = \infty$; M_0 , magnetization at $t = 0$; β , a free variable).

Table S7. The best fitting results for dc magnetic relaxation data for **1** under 1200 Oe applied dc field.

T (K)	M_0/M_0	M_f/M_0	τ (s)	β
2	1.02108	0.61588	2002.67819	0.30643
3	1.01020	0.41325	1701.440	0.41520
5	0.97970	0.06081	753.07138	0.67376
6.25	1.00584	0.06703	198.10346	0.73986
8	1.01760	0.07434	54.2002	0.79894
11	1.00421	0.15698	12.25133	0.87192
15	1.00008	0.63899	3.01431	0.86666

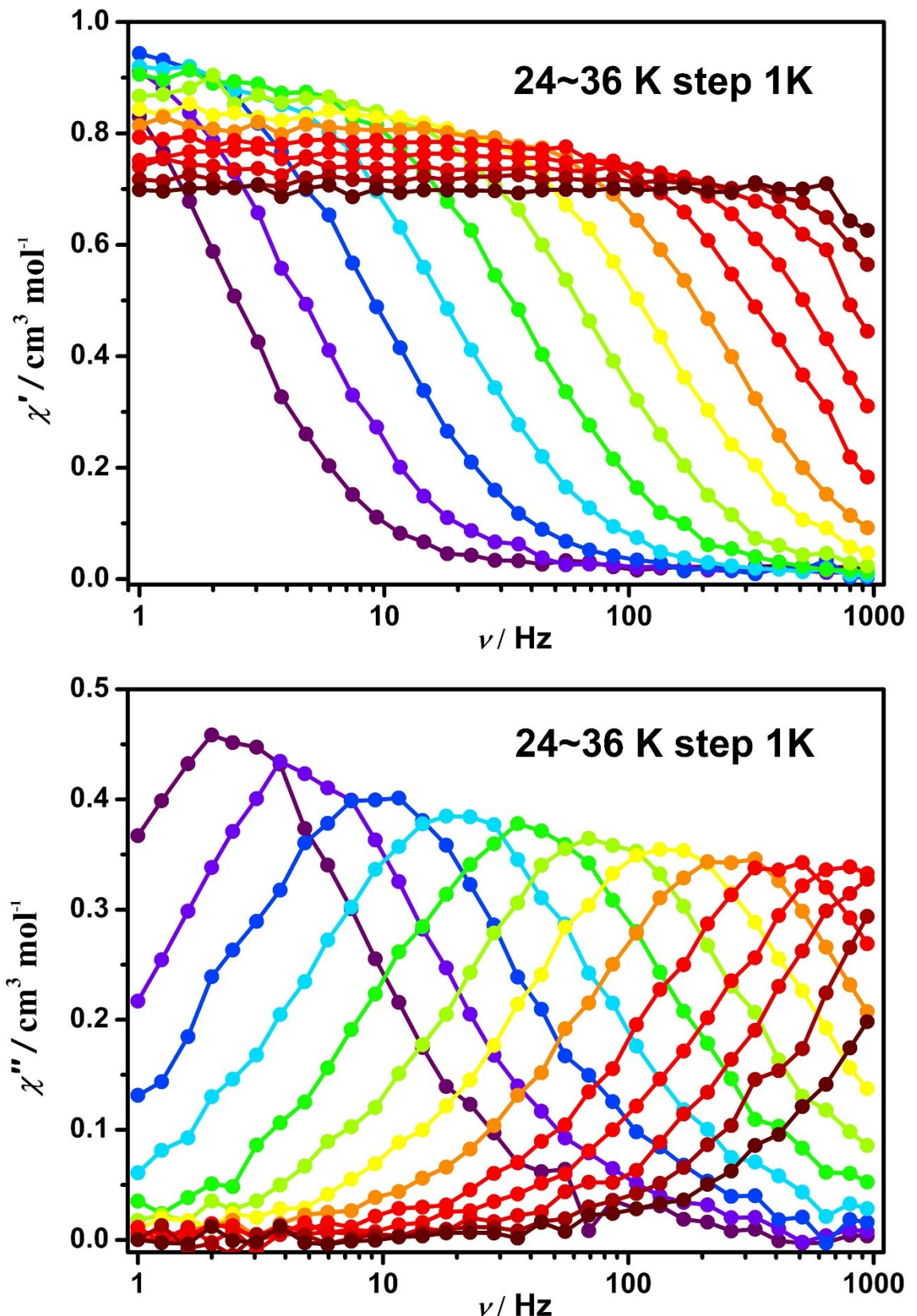


Fig S10. In-phase (top) and put-of-phase (bottom) components of variable-frequency ac susceptibility of **1@Y** under zero dc field.

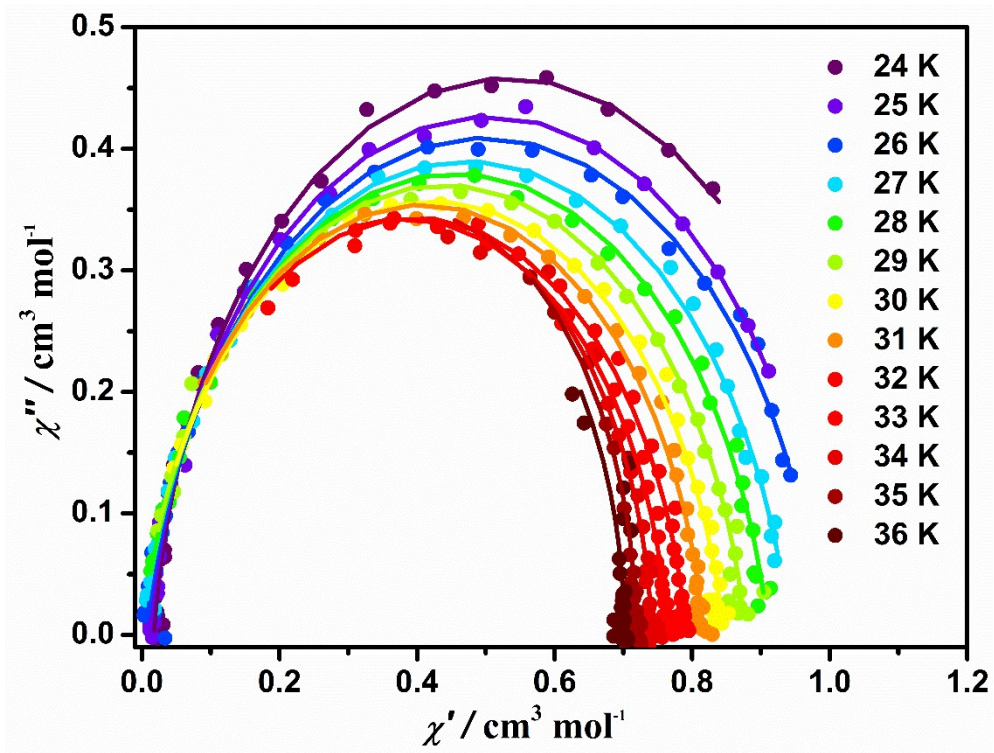


Fig S11. Cole-Cole plots for **1@Y** under zero dc field. The solid lines represent the best fitting results using Debye mode.

Table S8. The best fitting parameters for Cole-Cole plots of **1@Y** under zero applied dc field

T (K)	χ_s	χ_t	τ (s)	α
24	0.0174151	1.04432	0.0687094	0.0723027
25	0.0109649	0.997467	0.0346205	0.0921045
26	0.00521581	0.98864	0.0175952	0.116606
27	0.00115185	0.942075	0.00839536	0.118721
28	4.9165E-4	0.911204	0.00416077	0.114785
29	9.61294E-9	0.878219	0.0021356	0.107779
30	1.82644E-8	0.845336	0.00112449	0.106629
31	1.61992E-8	0.816794	6.31646E-4	0.0905478
32	3.04684E-8	0.791316	3.53297E-4	0.0897982
33	4.56221E-9	0.764765	2.1081E-4	0.0695049
34	7.78275E-9	0.741249	1.31219E-4	0.0349722
35	1.55545E-8	0.71838	8.70765E-5	2.2123E-16
36	2.42841E-8	0.701336	5.3029E-5	2.26028E-16

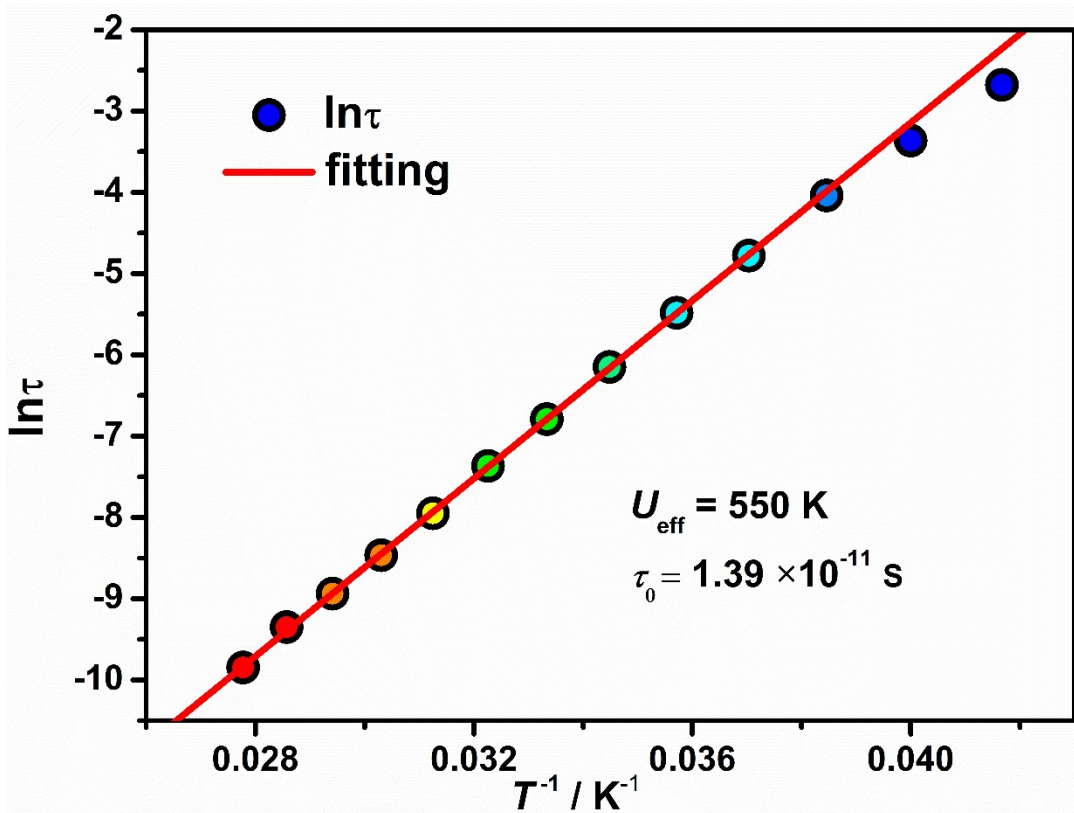


Fig S12. Plot of $\ln\tau$ versus T^{-1} of **1@Y** under zero dc field. The solid lines represent the best fitting results using Arrhenius law.

4. References

- [1] (a) H. Zabrodsky, S. Peleg and D. Avnir, *J. Am. Chem. Soc.*, 1992, **114**, 7843; (b) M. Pinsky and D. Avnir, *Inorg. Chem.*, 1998, **37**, 5575
- [2] Y.-C. Chen, J.-L. Liu, L. Ungur, J. Liu, Q.-W. Li, L.-F. Wang, Z.-P. Ni, L. F. Chibotaru, X.-M. Chen, M.-L. Tong, *J. Am. Chem. Soc.*, 2016, **138**, 2829
- [3] S. K. Gupta, T. Rajeshkumar, G. Rajaraman, R. Murugavel, *Chem. Sci.*, 2016, **7**: 5181.
- [4] Y.-C. Chen, J.-L. Liu, Y.-H. Lan, Z.-Q. Zhong, A. Mansikkamaki, L. Ungur, Q.-W. Li, J.-H. Jia, L. F. Chibotaru, J.-B. Han, W. Wernsdorfer, X.-M. Chen, M.-L. Tong, *Chem. Eur. J.*, 2017, **23**, 5708.
- [5] A. B. Canaj, M. K. Singh, C. Wilson, G. Rajaraman, M. Murrie, *Chem. Commun.*, 2018, **54**, 8273.